A 6 MJ spherical hohlraum target for heavy ion inertial fusion

M.M. Basko*

Département de recherches sur la fusion contrôlée,
CEA Cadarache,
St.-Paul-lez-Durance,
France

Abstract. A new target option for energy applications of heavy ion inertial fusion is analysed. It has a spherical hohlraum and is irradiated by ion beams along the directions of the zeros of the fourth Legendre polynomial P_4. The target performance is simulated with a 1-D three temperature hydrodynamics code and with a 2-D view factor code. Its efficiency is shown to depend crucially on the structure of the hohlraum wall, which, simultaneously, plays the role of the X ray converter. For an optimized pulse power profile, a 1-D energy gain of $G = 78$ is calculated with an input energy of $E_{dr} = 6.1$ MJ in the form of 5 GeV ^{209}Bi ions focused on the target sphere with an outer radius of $R = 6.37$ mm.

1. Introduction

Heavy ion accelerators are considered as a leading driver option for inertial fusion energy (IFE) because of their high efficiency and repetition rate [1, 2]. In a coherent concept of a heavy ion fusion (HIF) facility, the target design should match the accelerator capabilities in terms of such key parameters as the ion energy, the focal spot size, the number and spatial geometry of irradiating beams, and the peak value and temporal profile of the power pulse. Clearly, when different options for the accelerator and final focus designs are considered and assessed, it is also important to have a choice from several target options to be able to find an optimized overall solution. The purpose of this article is to present a possible type of HIF target aimed at IFE applications that has not been discussed in the literature before.

Recently Tabak et al. [3] proposed an indirect drive target with a cylindrical hohlraum suitable for two sided illumination by heavy ion beams. With a driver energy of $E_{dr} = 6.5$ MJ in the form of 3 GeV (foot of the pulse) and 4 GeV (main pulse) lead ions, focused on two 5 mm radius spots, they calculated an energy gain of $G = 66$ in 2-D integrated simulations with the LASNEX code. This target has a rather complex 2-D structure, and its performance can only be evaluated with a 2-D radiation hydrodynamics code. The calculated gain value is high enough to fulfil the condition $G\eta_{dr} \geq 10$ for energy applications when the driver efficiency $\eta_{dr} \geq 0.20$–0.25.

At the same time, the recently completed HIDIF study [4] has been conducted for 10 GeV, $A \approx 200$ ions with the original goal of laying out a concept for a heavy ion ignition facility. Its driver is based on a radiofrequency linear accelerator with storage rings and a ballistic final focusing. Because of a longer ion range, the HIDIF targets use compact (rather than distributed as in Ref. [3]) X ray radiators (converters) with focal spot radii of $r_f \approx 1.7$ mm. The two main target options considered — one with two X ray converters and radiation screens inside the hohlraum, and the other with eight converters and no radiation screens — both employ cylindrical hohlraums. Aimed at minimizing the ignition energy, these targets have been evaluated to produce rather low energy gains of $G = 3$–5 at $E_{dr} = 3$–4 MJ. Neither of them appears to scale favourably to the IFE energy level.

One of the results of the HIDIF study was a large number (48) of individual beam lines which, passing through space demanding arrays of final focus magnets, converge on a target with a considerable spread (of up to $\pm 30°$) of the incidence angles. Under such conditions, a natural alternative to the two sided ion illumination would be a 4π (quasi-spherical) illumination geometry. The main objection to this option has always been the extra costs associated with steering the rigid ion beams at considerable angles with respect to the horizontal plane. These costs, however, may be more than offset by the advantages

* *On leave from:* Institute for Theoretical and Experimental Physics, Moscow, Russian Federation.

 ©1999, IAEA, Vienna

of a simpler target design and relaxed requirements on the final focal spot. The 4π illumination geometry opens the possibility of employing spherical hohlraums, which, in general, are more efficient than cylindrical ones.

In this article, we explore a reactor scale HIF target with a spherical hohlraum approximately twice the size of the fusion capsule. The capsule, taken from Ref. [5], is driven by the X ray radiation generated along the entire inner surface of the hohlraum case. In this sense our target has a distributed X ray radiator. The low asymmetry modes ($l < 8$) are suppressed by directing the ion beams along the zeros of the fourth Legendre polynomial P_4 (hence the name 'P4 target' used below), i.e. approximately at angles ± 20 and $\pm 60^\circ$ with respect to the horizontal plane. The target performance is investigated with the 1-D three temperature (3-T) hydrodynamics code DEIRA [6] and the 2-D view factor code VF2 [7]. With an input energy of $E_{dr} = 6.1$ MJ in the form of 5 GeV bismuth ions, a 1-D energy gain of $G = 78$ is calculated. The focal spot is essentially the whole target cross-section with a radius of $R \approx 6$ mm.

The idea of using a spherical hohlraum irradiated by particle beams over a significant fraction of 4π steradians is not new and has been discussed in the context of light ion fusion [8, 9] and HIF [10]. As contrasted to the 'hotraum' target of Ref. [10], the present P4 target has a more realistic fusion capsule, which requires a much longer and carefully tailored power pulse; this, in turn, implies a more complex hohlraum dynamics. An important issue becomes the structure of the ion absorbing layer.

Compared with the distributed radiator target of Ref. [3], our P4 target has the advantage of a much simpler overall structure. Having approximately the same focal spot size, it is driven by ions with a higher and single energy value of 5 GeV, which is beneficial for the accelerator design. The disadvantage is a more complex and potentially more costly spatial beam arrangement. Our calculated energy gain of $G = 78$ is also somewhat higher than that of Ref. [3]. It can be expected that the full 2-D simulations confirm the 1-D thermonuclear yield, provided that certain small modifications (such as, e.g., the variable thickness of the outer gold layer mentioned in Section 4) are perhaps introduced to ensure the uniformity of the radiation field in the hohlraum. The energy gain may, however, decrease to a certain extent because of a less efficient beam to radiation energy conversion when the finite spread of the ion trajectories over the incidence angles is taken into account in two and three dimensions.

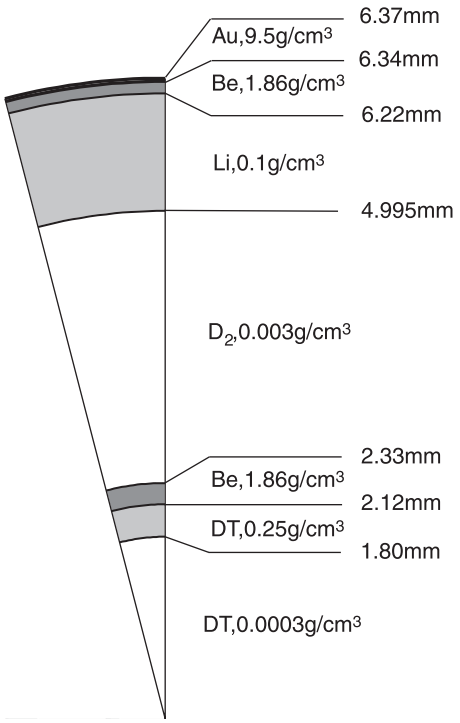

Figure 1. Initial configuration and parameters of the spherical P4 target used in 1-D simulations.

2. Basic target parameters and ion energy

The fusion capsule for the present study is taken from Ref. [5] and its parameters are given in Fig. 1. When isolated from the hohlraum enclosure and simulated with the DEIRA code, it requires about 1.1 MJ of the radiation energy to be driven to ignition and produces some 420 MJ of thermonuclear yield. Its main performance characteristics are close to those listed in Table I of Ref. [11], except that the radiation temperature peaks at 215 eV instead of 260 eV when a pure beryllium ablator is used.

To demonstrate an energy gain of $G \simeq 50$ that would be of interest for energy applications, a target with a fusion yield of $Y \simeq 400$ MJ should be driven by $E_{dr} \lesssim 7$ MJ of the ion energy. Then, we are left with less than 6 MJ to heat the X ray converter up to its 'working' temperature of $\simeq$250 eV. For a beryllium converter this implies an upper limit of $M_{con} \lesssim 200$ mg for its total mass

$$M_{con} = 4\pi R^2 \langle \rho l \rangle_i \qquad (1)$$

which is supposed to be spread evenly along the inner surface of the spherical hohlraum case (Fig. 1). Here R is the target (hohlraum) radius and $\langle \rho l \rangle_i$ is the range (in g/cm^2) of irradiating ions in beryllium.

To ensure adequate symmetrization of the radiation flux on the capsule and to avoid hydrodynamic coupling between the converter and the imploding fuel, the hohlraum radius R should be at least a factor of 2 larger than the capsule radius $R_c = 2.33$ mm. When combined, the constraints of $R \gtrsim 5$ mm and $M_{con} \lesssim 200$ mg result (by virtue of Eq. (1) and the known relationship between $\langle \rho l \rangle_i$ and the ion energy E_i) in an upper limit of $E_i \lesssim 5.5$ GeV for the energy of irradiating heavy ions with $A \simeq 200$. On the other hand, for a hohlraum target driven by particle beams, when the hohlraum case has no beam entrance holes, there is an optimum value of the particle energy E_i determined by the balance between the energy lost to heat up the converter (which dominates for too high values of E_i) and the radiation loss to the outside (which dominates for too low values of E_i). According to the simulations of Ref. [10], this optimum is close to $E_i = 5$–7 GeV for our conditions.

The above considerations provide a general explanation for the choice of principal target parameters and the ion energy, which was fixed at a value $E_i = 5$ GeV for ^{209}Bi ions in all the simulations described below. The overall target structure is shown in Fig. 1. The initial density of the deuterium hohlraum fill was fixed at a value of 0.003 g/cm^3, which, on the one hand, is low enough to allow a rapid radiative burnthrough and, on the other hand, is sufficiently high to provide protection against a low energy tail of irradiating ions beyond the Bragg peak. More details on specific aspects of the target structure are given in the corresponding sections below.

3. Illumination geometry

In a spherical hohlraum with a concentric capsule, a spherical mode l, m of the source brightness perturbation on the hohlraum wall generates the same l, m harmonic on the capsule [12, 13]. Hence, the ion beams should be positioned so as to eliminate the maximum number of low modes in the non-uniformity of the energy flux on the target surface. In particular, special care should be taken of the $l = 2$ and 4 modes in a tight hohlraum with $R/R_c \lesssim 3$.

Here we assume that the illumination pattern is symmetric with respect to the horizontal plane

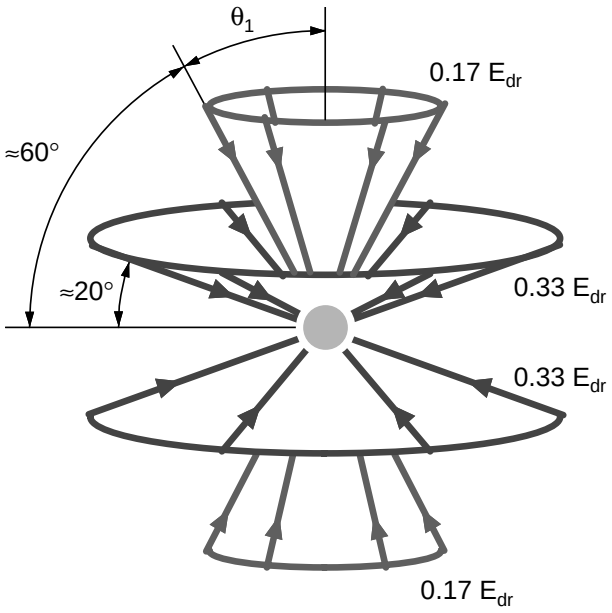

Figure 2. Illumination geometry of the P4 target: ion beams approach the target in two cones at angles corresponding to the zeros of the fourth Legendre polynomial P_4.

(which implies that all the modes with uneven l vanish), and that in each hemisphere there are two cones of azimuthally equally spaced ion beams: N_1 beams in the inner cone at a polar angle θ_1 (with respect to the vertical axis, Fig. 2) and N_2 beams in the outer cone at a polar angle θ_2. The three 'meridional' free parameters of this illumination scheme, namely, the angles θ_1, θ_2 and the power ratio W_1/W_2 between the two cones, can be chosen such as to eliminate the $l = 2$, 4, and 6 modes with $m = 0$ [2]. The lowest non-vanishing m modes depend on the values of N_1 and N_2.

To perform the quantitative analysis, we expand the ion irradiation intensity

$$F(\phi, \theta) = a_{00}\left(Y_{00} + \sum_{l=1}^{\infty} \sum_{m=-l}^{+l} \bar{a}_{lm} Y_{lm}(\phi, \theta)\right) \qquad (2)$$

in terms of the normalized spherical harmonics

$$Y_{lm}(\phi, \theta) = \frac{1}{\sqrt{2\pi}}\, e^{im\phi} \Theta_{lm}(\theta). \qquad (3)$$

To evaluate the dimensionless amplitudes $\bar{a}_{lm}$, we assume that each ion beam produces the same azimuthally symmetric normalized flux intensity

$$f(\gamma) = 1 + \sum_{l=1}^{\infty} f_l P_l(\cos\gamma) \qquad (4)$$

on the target surface; here γ is the polar angle with respect to the corresponding beam axis. Similarly to Ref. [14], we calculate

$$\bar{a}_{lm} = \frac{\sqrt{2}}{W_1 + W_2} \frac{f_l}{2l+1} \sum_{j=1}^{2} \beta_{mN_j} W_j e^{-im\phi_j} \Theta^*_{lm}(\theta_j). \tag{5}$$

Here W_j is the total power in the beam cone j ($j = 1, 2$), ϕ_j is the azimuth of the first of the N_j beams in cone j,

$$\beta_{mN_j} = \begin{cases} 1, & m = 0, \ \pm N_j, \ \pm 2N_j, \ \ldots, \\ 0, & \text{otherwise}, \end{cases} \tag{6}$$

and the asterisk denotes a complex conjugate.

By virtue of Eq. (5) one readily verifies that $\bar{a}_{20} = \bar{a}_{40} = \bar{a}_{60} = 0$ when the values

$$\begin{aligned} \theta_1 &= \cos^{-1} \mu_{4,1} = 30.555^\circ \\ \theta_2 &= \cos^{-1} \mu_{4,2} = 70.124^\circ \end{aligned} \tag{7}$$

are chosen, and the power ratio is set equal to

$$\frac{W_1}{W_2} = -\frac{P_2(\mu_{4,2})}{P_2(\mu_{4,1})} = \frac{3\sqrt{6/5} - 1}{3\sqrt{6/5} + 1} \approx 0.5334. \tag{8}$$

Here

$$\mu_{4,(1)(2)} = \left[\frac{1}{7} \left(3 \pm 2\sqrt{\frac{6}{5}} \right) \right]^{1/2} \tag{9}$$

are the zeros of the $P_4(\mu)$ Legendre polynomial.

If the beam numbers N_j are large enough, namely $\geq$8, the lowest non-vanishing non-uniformity modes begin with $l = 8$. In reality, an acceptable uniformity may in fact be achieved with smaller numbers of beams, which would be an obvious advantage for the reactor chamber design. As an interesting possibility, one can consider the combination $N_1 = 4$, $N_2 = 6$, $\phi_1 = \phi_2 = 0$. In this case the lowest non-zero modes,

$$\bar{a}_{4\pm4} = 3.64 \times 10^{-2} \left(\frac{f_4}{9} \right), \quad \bar{a}_{6\pm4} = 0.21 \left(\frac{f_6}{13} \right) \tag{10}$$

are reduced by additional geometric factors of $\simeq$30 and $\simeq$5, respectively, as compared with the higher modes

$$\bar{a}_{6\pm6} = -0.77 \left(\frac{f_6}{13} \right), \quad \bar{a}_{80} = -1.20 \left(\frac{f_8}{17} \right). \tag{11}$$

Much depends on the width of individual beams, i.e. on the values of f_l (for needle-like beams $f_l = 2l+1$).

As a final remark, we note that the above analysis can only serve as a first approximation and a guide to the practical choice of illumination parameters. Due to non-linear effects in successive energy coupling stages, the values of θ_1, θ_2 and W_1/W_2 which minimize the low mode non-uniformity of the fuel implosion will generally differ somewhat from those given by Eqs (7) and (8). For accurate predictions of acceptable numbers and positions of the ion beams one will have to perform 3-D integrated radiation hydrodynamics simulations.

4. View factor simulations

To evaluate the non-uniformity of the radiation field along the surface of the fusion capsule, 2-D simulations with the view factor code VF2 [7] have been performed for a static spherical hohlraum with the case to capsule radial ratio $R/R_c = 2$. The 2-D limit of the 3-D illumination scheme described above corresponds to $N_1 = N_2 = \infty$. In the simulations, the beam cone angles θ_1, θ_2 and the power ratio W_1/W_2 between the two cones were set equal to the values given by Eqs (7) and (8). The radial profile of individual beams was assumed to be an inverted parabola, with the ion flux density at a distance r from the beam axis proportional to $1-(r/r_f)^2$, where r_f is the focal spot radius. The view factor results are not sensitive to the exact beam profile, and we have chosen the simplest non-rectangular shape of finite length in order not to deal with the beam losses in Gaussian-like tails.

Figure 3 shows the amplitude $|c_8|$ of the dominant P_8 mode in the angular expansion

$$\mathcal{E}_c(\theta) = \mathcal{E}_{c0} \left(1 + \sum_{l=1}^{\infty} c_l P_l(\cos\theta) \right) \tag{12}$$

for the total energy per unit surface area $\mathcal{E}_c$ (erg/cm^2) absorbed by the capsule by the end of the ion pulse as a function of the focal spot radius r_f. The Legendre 2-D amplitudes c_l are related to the spherical 3-D coefficients $\bar{a}_{lm}$ of the 3-D expansion for $\mathcal{E}_c(\phi, \theta)$ analogous to Eq. (2) as

$$c_l = i^l \sqrt{2l+1}\, \bar{a}_{l0}. \tag{13}$$

In our case, when the flux non-uniformity is strongly dominated by the single P_8 mode, the peak to valley (PTV) amplitude is very close (typically within a factor of 1.1–1.2) to $|c_8|$, whereas the root mean square (RMS) deviation practically coincides with $|\bar{a}_{80}| = |c_8|/\sqrt{17}$ because in general

$$\mathrm{RMS} = \left(\sum_{l,m} |\bar{a}_{lm}|^2 \right)^{1/2}. \tag{14}$$

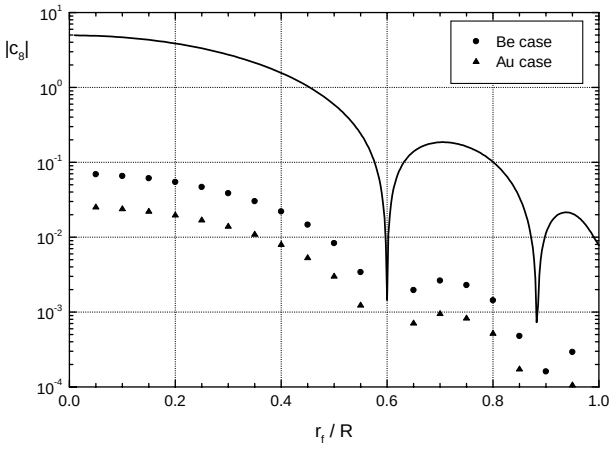

Figure 3. Absolute magnitude of the amplitude $|c_8|$ (as defined by Eq. (12) and calculated with the 2-D view factor code) of the dominant P_8 mode in the angular distribution of the radiation energy as a function of the ion beam focal radius r_f. Solid curve: non-uniformity of the source flux on the hohlraum wall. Circles (triangles): non-uniformity of the total energy absorbed by the fusion capsule in the case of a beryllium (gold) hohlraum wall.

Two sets of calculated points are shown in Fig. 3: one corresponding to the beryllium, and the other to the gold, hohlraum walls. For the sandwich-like structure shown in Fig. 1, the realistic case should lie between these two.

The results presented in Fig. 3 demonstrate that an adequate uniformity of capsule drive (PTV $< 1\%$) is obtained when the beam focal radius r_f is sufficiently large compared with the target radius R, namely, at $r_f/R > 0.5$. The precipitous drop of the P_8 amplitude around $r_f/R = 0.5$ indicates that the drive symmetry is sensitive to the presence of dark (not covered by the ion beams) spots on the hohlraum case: the dark spots at the target poles disappear for $r_f/R \geq 0.5$. In reality, this may mean that special care should be taken for a synchronous early burnthrough of the inner low density converter layer by, say, reducing the wall thickness at places where the average ion incidence angle deviates significantly from zero (as, e.g., on the target poles).

5. X ray converter design

The outer wall of our target serves a double purpose: on the one hand, it absorbs the ion beams and converts their energy into thermal radiation; on the other hand, it confines this radiation inside the hohlraum. As will be shown below, the overall target performance is quite sensitive to the structure of this wall. The general strategy in designing such an enclosure–converter wall is to deposit the largest possible fraction of the beam energy in a low-Z converter layer, covered from the outside by a thin layer of high-Z material which minimizes the outward radiation loss. In our case the optimum thickness of the high-Z protective layer corresponds to some 15 μm of solid density gold (a somewhat better choice would be a 50:50 alloy of gold and gadolinium because of a higher combined opacity [15]): it absorbs about 20% of the 5 GeV ion energy and lets some 5–10% of the total energy leak out of the hohlraum. Here we use a 30 μm layer of the 9.5 g/cm^3 gold foam, which performs slightly better than the solid gold with regard to the hydrodynamic expansion.

Besides efficiency of conversion into X rays, the key factor which dictates the structure of the converter layer is the intensity of its expansion into the hohlraum. The converter expansion becomes an acute problem for our target because of the necessity to combine a relatively long (about 20 ns, see Fig. 6) foot of the ion pulse, required to drive a low entropy first shock through the fuel layer, with a relatively tight hohlraum. If the converter expands too quickly too early, the target performance is strongly degraded (or ruined altogether), for one reason, because of a too strong and too early second shock generated by the secondary burst of X rays (for more details see the next section) and, for another reason, because of the pressure non-uniformities propagating from the ion deposition region into the fuel. Hence, our task is to achieve maximum radiation output with minimum hydrodynamic motion of the converter material.

The best material for converting ion energy into radiation with temperatures $T_r = 100$–300 eV is either lithium or beryllium. These two elements possess the best combination of the equation of state and stopping power, which minimizes the energy spent in heating the converter to its 'working' temperature [16]. In our case it is advantageous to have a double layer converter, with a lithium layer facing the hohlraum and a beryllium layer at its rear side (Fig. 1). There are two physical reasons for this, namely, the X ray temperature variation during the power pulse and the effect of ion range shortening. During the foot of the pulse, lithium is a better radiator because the beryllium opacity is too high for efficient emission of X rays with $T_r = 80$–100 eV. The thicknesses of the lithium and beryllium layers are adjusted such that the ions stop initially (at $t = 0$)

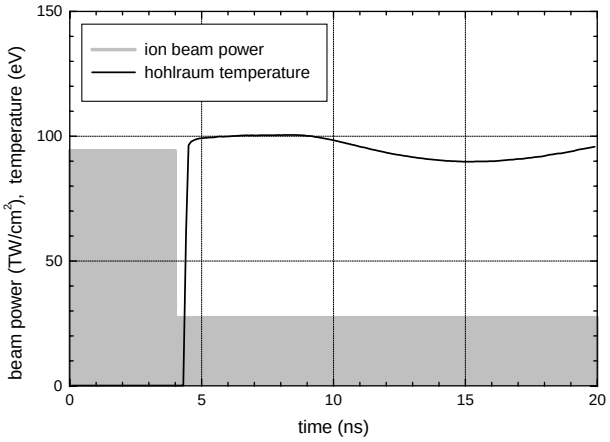

Figure 4. Temporal history of the radiation temperature in the middle of the hohlraum (solid curve) calculated with the step-like pulse profile (shaded area) in case 3 of the X ray converter study (Table 1).

Table 1. Three cases of the X ray converter performance as described in the text

	Case 1	Case 2	Case 3
$\mathcal{E}_{dr}$ (MJ/cm^2)	1.35	1.58	0.81
$\mathcal{E}_{con,k}$ (MJ/cm^2)	0.33	0.40	0.15
$\mathcal{E}_{h,w}$ (MJ/cm^2)	0.13	0.15	0.020
Δr_{con} (mm)	4.9	5.2	2.3

at the lithium–hohlraum interface, and the ion penetration front recedes into the beryllium layer by the time the main pulse arrives.

The structure of the X ray converter was optimized by performing a separate series of 1-D DEIRA runs. In this series the radii of the capsule and the hohlraum were multiplied by a factor of 4, and a truncated ion pulse, shown in Fig. 4, was used. The thicknesses of the constituent material layers and the ion energy of 5 GeV were left unchanged. By increasing fourfold the hohlraum size we delay the collision between the expanding converter and the capsule ablator, so that the resulting secondary burst of X rays does not interfere with the primary conversion process.

Table 1 compares three characteristic cases of the converter performance. In cases 1 and 2 a single layer of solid beryllium was used, whereas case 3 corresponds to the double layer Li–Be structure shown in Fig. 1. In case 1 no ion range variations (with respect to the mass co-ordinate) with changing plasma parameters were allowed. In all three cases, a step-like (three steps in cases 1 and 2, and two steps in case 3) ion pulse, shown in Fig. 4, was adjusted to produce a ≈15 ns long pulse of $T_r \approx 100$ eV thermal X rays emitted into the hohlraum with a fixed radiation output of $\mathcal{E}_r = 0.05$ MJ/cm^2 by $t = 20$ ns.

By comparing case 2 with case 1 one sees how the effect of range shortening intensifies the converter expansion. For the same amount of radiation output, $\mathcal{E}_r = 0.05$ MJ/cm^2, one needs 17% more beam energy $\mathcal{E}_{dr}$ in case 2, which augments correspondingly the kinetic energy $\mathcal{E}_{con,k}$ of the expanding converter and the amount of the PdV work $\mathcal{E}_{h,w}$ against the hohlraum fill.

Case 3 manifests a dramatic improvement against cases 1 and 2: the required beam energy $\mathcal{E}_{dr}$ goes down by about a factor of 2, the converter kinetic energy $\mathcal{E}_{con,k}$ decreases by a factor of 2–2.5 and the PdV work $\mathcal{E}_{h,w}$ falls by about a factor of 7. The displacement of the converter–hohlraum interface during the first 20 ns, Δr_{con}, is reduced by more than a factor of 2. This improvement is due primarily to a low initial density 0.1 g/cm^3 of the front converter layer. The fact that this foam layer is made of lithium rather than of beryllium is not very important: it only improves the performance characteristics in Table 1 by some 10%.

There are two main physical reasons behind the strong reduction of the converter expansion in case 3. The first has a pure hydrodynamic origin and has already been explained in Ref. [11]. If one heats the same column density of the converter material to the same temperature, but in one case as a single solid density layer, and in the other with a low density cushion between the main converter body and the hohlraum, the converter in the second case expands less violently and generates lower stagnation pressures when collided with the expanding capsule ablator.

The second reason is due to the non-uniformity of the ion energy deposition and opacity profiles, and is illustrated in Fig. 5. Firstly, the Bragg peak in the ion deposition profile is significantly enhanced in the lithium layer during the first few nanoseconds because of the low initial density (see curve 0.5 ns in Fig. 5). Secondly, the lower opacity of this layer makes it a more efficient radiator of the 80–100 eV thermal X rays than the initially solid beryllium. As a consequence, the same radiative power is generated by about a factor of 2 lower ion beam power, which, in its turn, results in about a factor of 2 lower temperature of the converter interior during the first 10–15 ns (see the T_e curves for 5 and 10 ns in Fig. 5).

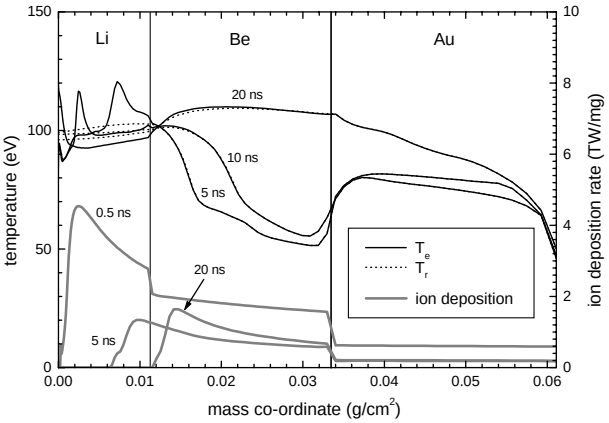

Figure 5. Profiles of the electron (solid curves) and radiation (dotted curves) temperatures and of the specific ion energy deposition rate (thick grey curves) at three characteristic times in case 3 of the X ray converter study.

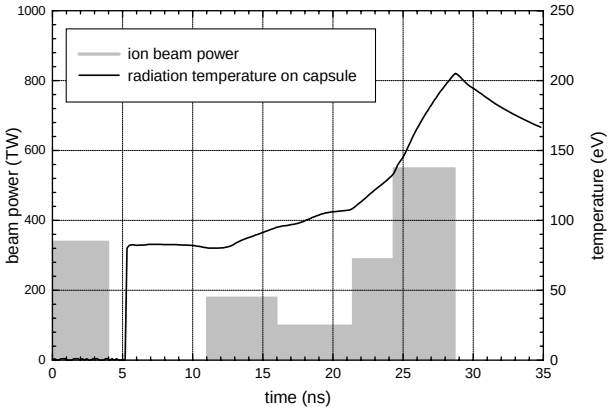

Figure 6. Optimized ion power pulse (shaded area) which leads to the target energy gain of $G = 78$. The solid curve shows the evolution of the radiation temperature at the surface of the fusion capsule.

A strong temperature dip inside the beryllium layer means a considerably lower pressure to push the converter into the hohlraum. Later on, when the main pulse arrives at $t > 20$ ns and the temperature rises above 200 eV, the ion deposition profile has already receded into the beryllium layer (which may need some doping by a heavy element to optimize the opacity), and the optically thin lithium layer does not become overheated. In this way we employ the effect of ion range shortening to enhance the radiative efficiency and reduce the hydrodynamic motion of the X ray converter during the foot of the radiation pulse.

6. Hohlraum dynamics and overall target performance

Efficient target performance depends strongly on careful tailoring of the ion power pulse, aimed at driving the fuel implosion along the lowest possible adiabat. The optimized pulse profile, which results in a thermonuclear yield of $Y = 471$ MJ for $E_{dr} = 6.06$ MJ of beam energy, is shown in Fig. 6 as a grey shaded area. The choice of a stepwise function has no particular significance. The initial 4 ns prepulse of 340 TW 'warms up' the hohlraum and launches the first 1.2 Mbar shock front into the DT. Then, essentially no additional beam power is needed to maintain the hohlraum temperature at $T_r = 80$–90 eV for more than 20 ns: it is the dissipation of the converter and ablator kinetic energy which feeds the hohlraum heat bath. The main pulse, starting at $t = 11$ ns and culminating with the peak power of 550 TW during the last 4.4 ns, is tailored to minimize the entropy generated in the solid DT layer by the second and the third shock fronts.

The radiation temperature in the hohlraum (solid curve in Fig. 6) peaks at 205 eV. In our 3-T diffusion treatment of the radiation transport the opacity of natural beryllium was found to be adequate for efficient converter and capsule performance at this temperature. On the other hand, the earlier results from LASNEX simulations [17], obtained with a more realistic opacity model and radiation transport scheme, indicate that the optimized converter performance may require a high-Z dopant to be added to the natural beryllium in order to increase its opacity, which would allow excessive temperatures and pressures to be avoided in beryllium during the peak of the power pulse. (In our simulations, even when the beryllium layer becomes somewhat overheated, the excessive heat is quickly radiated into the hohlraum 1–2 ns later.) However, such a rectification would be premature at the present stage and was not attempted in this work. Similarly, a high-Z (or medium-Z) dopant may be needed in the beryllium ablator of the fusion capsule to shield the fuel from hard X rays (not described by our 3-T model) and to fine tune the implosion dynamics, as demonstrated in Ref. [18]. A thermonuclear yield 10% higher than that in Ref. [5], calculated here for the same capsule, appears to be due to the fact that a thin crust of unablated beryllium (8% of the initial beryllium mass) is left around the DT shell, which provides some extra confinement during the thermonuclear flare as compared with the fully ablated case.

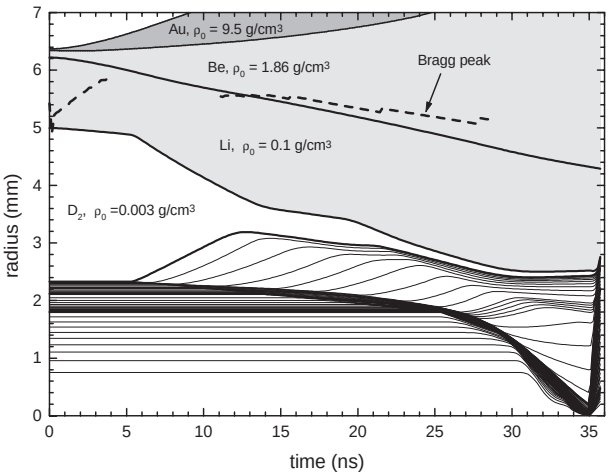

Figure 7. Radius–time diagram of the dynamics of the P4 target, whose initial configuration is shown in Fig. 1. The dashed line shows the position of the maximum on the ion energy deposition curve — the Bragg peak (cf. grey curves in Fig. 5).

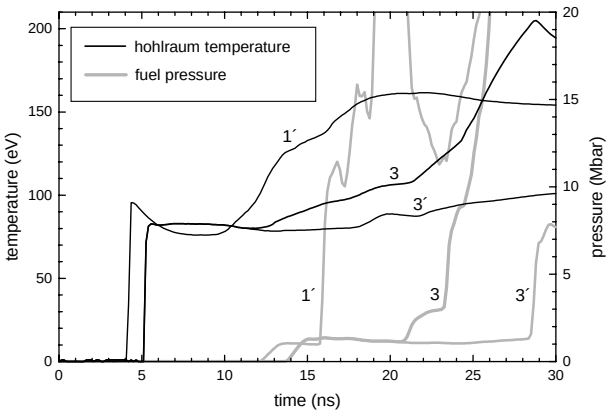

Figure 8. Evolution of the radiation temperature at the capsule surface (solid curves, left-hand ordinates) and of the pressure at the fuel–ablator interface (grey curves, right-hand ordinates) in three cases of the target performance. Case 1′, the lithium foam layer (Fig. 1) is replaced by an equivalent layer of solid beryllium, a 970 TW ion pulse is terminated at $t = 4$ ns. Case 3′: the target structure is as shown in Fig. 1, a 340 TW ion pulse is terminated at $t = 4$ ns. Case 3 (a reference case): full target performance with the ion pulse shown in Fig. 6.

Figure 7 shows the r–t diagram of the overall target dynamics. At about $t = 13$ ns the ablated beryllium of the fusion capsule collides with the expanding lithium layer of the converter. The collision generates pressures comparable to the ablation pressure and launches a shock wave, which propagates inwards into the blowing out capsule material. However, as is clearly seen in Fig. 7, this shock front never reaches the imploding fuel. This means that no hydrodynamic contact is established between the ion deposition region and the DT fuel.

The X ray emitting region is primarily associated with the Bragg peak on the ion deposition curve, whose position is indicated by a dashed curve in Fig. 7. Because of the range shortening in the hot expanding converter plasma the Bragg peak never advances into the hohlraum beyond its initial position at $r \approx 5.2$ mm. Hence, the separation between the capsule surface and the X ray radiator is always in excess of one capsule radius, which should guarantee an adequate symmetry of radiation drive on the capsule.

At $t = 32$ ns, when the DT shell implodes to approximately one half of its initial radius, it reaches the implosion velocity of $v_{im} = 2.6 \times 10^7$ cm/s. At this moment about 90% of the fuel mass has a value of the α parameter (defined as the ratio between the actual pressure P and the pressure P_{deg} of fully degenerate electrons at the same density) below 1.1. Note that values of α below 1 are possible because of the departure of the DT equation of state from that of a fully ionized ideal gas.

The successful performance of our target, as described above, depends crucially on the presence of a low density lithium (or beryllium) foam layer on the inside of the X ray converter. To demonstrate this quantitatively, two separate computer runs have been performed for the initial stage driven solely by the initial 4 ns prepulse in two different cases. Case 3′ in Fig. 8 corresponds to the target structure exactly as it is shown in Fig. 1, but with the ion pulse (Fig. 6) truncated at $t = 4$ ns. In case 1′ the lithium foam was replaced by an equivalent (with respect to the ion stopping) layer of 1.86 g/cm^3 beryllium, and the power of the initial 4 ns prepulse was increased to 970 TW to reach the hohlraum temperature of 80–90 eV needed to launch a ∼1 Mbar first shock wave into the DT shell; the ion range was kept fixed with respect to the mass co-ordinate. In terms of the converter structure, cases 1′ and 3′ correspond, respectively, to cases 1 and 3 in Table 1.

Case 1′ demonstrates clearly that, when the converter has no foam lining from inside, one actually loses control over the timing and intensity of the second shock wave in the fuel. Figure 8 compares the temporal history of the hohlraum temperature and fuel pressure in cases 1′ and 3′; the

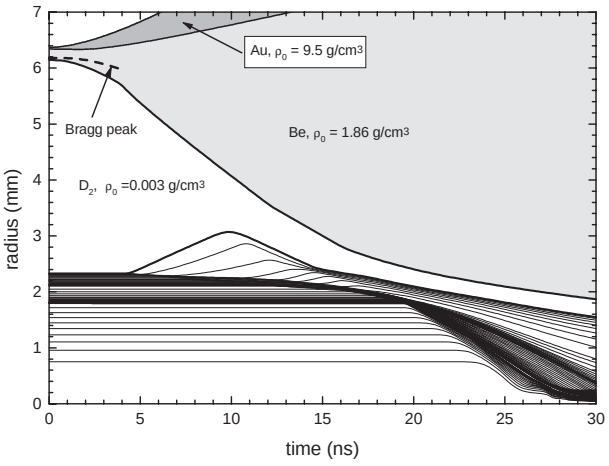

Figure 9. Same as Fig. 7 but for the case 1′ of the target performance.

hohlraum dynamics for case 1′ is shown in Fig. 9. At $t \geq 10$ ns the collision between the expanding ablator and converter layers (some 2 ns earlier than in case 3′) generates a strong burst of secondary X rays, which manifests itself as a steep rise of the hohlraum temperature to 130–140 eV between $t = 10$ ns and $t = 14$ ns (Fig. 8). This additional radiation drives a second shock wave into the fuel much too early (at $t = 16$ ns, see the dashed grey curve 1′ in Fig. 8) and much too strong. Note that in case 3′ the secondary X ray radiation becomes only hardly noticeable at $t > 20$ ns, when it is already of no significance for the capsule drive.

In Figs 8 and 9 one sees that the pressure wave from the ablator–converter collision reaches the fuel at $t = 19$ ns. On the one hand, this confirms the fact that the second shock, launched some 3 ns earlier, is generated by radiation rather than by direct hydrodynamic push. On the other hand, it means that a direct hydrodynamic contact is established between the converter and the fuel after $t = 19$ ns. As a result, the symmetry of the fuel implosion is likely to be destroyed by non-uniformity of the ion deposition during the main ion pulse. Finally, it should be noted that these negative factors are only aggravated once full account is taken of the effect of ion range shortening in a single layer solid beryllium converter.

7. Conclusion

When the accelerator design points to a solution with many beam lines converging on target over a considerable solid angle — as, for example, in the HIDIF study [4] — a target with a 4π illumination geometry and a spherical hohlraum may become an attractive option. As a possible example, a 6 MJ target irradiated by ion beams directed along the zeros of the P_4 Legendre polynomial has been studied here. Static 2-D view factor simulations indicate that an adequate symmetry of radiation drive and fuel implosion can be achieved for a case to capsule radial ratio $R/R_c \geq 2$, provided that the ion beams illuminate the entire target surface, i.e. the focal spot radius r_f exceeds $0.5R$.

The focus of this work has been on the X ray converter structure and on the 1-D analysis of the target performance. It is demonstrated how the effect of ion range shortening can be employed to diminish the converter expansion and boost the target efficiency. The key element of the hohlraum design is a low density (0.1 g/cm^3) lithium (or beryllium) lining of the enclosure wall. For an optimized power profile, 1-D hydrodynamic simulations predict an energy gain of $G = 78$ for an input energy of $E_{dr} = 6.1$ MJ in the form of 5 GeV ^{209}Bi ions. These results should be considered as a first encouraging step which warrants further more detailed study of this type of heavy ion target by using more sophisticated tools (such as 2-D and 3-D radiation hydrodynamics codes), in view of its potential applications for fusion energy. Evidently, the ion beam arrangement proposed here is more complex than the two sided illumination and poses new problems for the reactor chamber design. It remains to be investigated whether the advantages of the target design and performance outweigh the additional difficulties for the chamber, and how the driver and final focus systems can be adapted to this quasi-4π illumination geometry.

Acknowledgements

The author is grateful to I. Hofmann and T. Mehlhorn for stimulating discussions.

References

[1] Arnold, R.C., Meyer-ter-Vehn, J., Rep. Prog. Phys. **50** (1987) 559.
[2] Lindl, J., Phys. Plasmas **2** (1995) 3933.
[3] Tabak, M., Callahan-Miller, D., Ho, D.D.-M., Zimmerman, G.B., Nucl. Fusion **38** (1998) 509.
[4] The HIDIF-Study, Report of the European Study Group on Heavy Ion Driven Inertial Fusion for the period 1995–1998, Rep. GSI-98-06, Gesellschaft für Schwerionenforschung, Darmstadt (1998).

[5] Ho, D.D.-M., Harte, J.A., Tabak, M., Nucl. Fusion **35** (1995) 1125.
[6] Basko, M.M., Nucl. Fusion **30** (1990) 2443.
[7] Basko, M., Phys. Plasmas **3** (1996) 4148.
[8] Imasaki, K., et al., Jpn. J. Appl. Phys. **23** (1984) L83.
[9] Mehlhorn, T., paper presented at European Advanced Research Workshop on Intense Ion Beams and Target Physics for Particle Driven ICF, Les Houches, 1995.
[10] Basko, M.M., Meyer-ter-Vehn, J., Nucl. Fusion **33** (1993) 601.
[11] Tabak, M., Callahan-Miller, D., Phys. Plasmas **5** (1997) 1895.
[12] Murakami, M., Nishihara, K., Jpn. J. Appl. Phys. **25** (1986) 242.
[13] Caruso, A., Strangio, C., Nucl. Fusion **31** (1991) 1399.
[14] Skupsky, S., Lee, K., J. Appl. Phys. **54** (1983) 3662.
[15] Orzechowski, T.J., et al., Phys. Rev. Lett. **77** (1996) 3545.
[16] Basko, M.M., Churazov, M.D., Koshkarev, D.G., Fusion Eng. Des. **32&33** (1996) 73.
[17] Ho, D.D.-M., Lindl, J.D., Tabak, M., Nucl. Fusion **34** (1994) 1081.
[18] Dittrich, T.R., Haan, S.W., Marinak, M.M., Pollaine, S.M., McEachern, R., Phys. Plasmas **5** (1998) 3708.

(Manuscript received 1 March 1999
Final manuscript accepted 14 June 1999)

E-mail addresses of M.M.Basko:
basko@drfc.cad.cea.fr, basko@vitep5.itep.ru

Subject classification: L0, It